ACS APPLIED MATERIALS & INTERFACES

Research Article

Cite This: *ACS Appl. Mater. Interfaces* 2019, 11, 33390−33398

www.acsami.org

Plasmonic WS_2 Nanodiscs/Graphene van der Waals Heterostructure Photodetectors

Mohammed Alamri,* Maogang Gong, Brent Cook, Ryan Goul, and Judy Z. Wu*

Department of Physics and Astronomy, University of Kansas, Lawrence, Kansas 66045, United States

Supporting Information

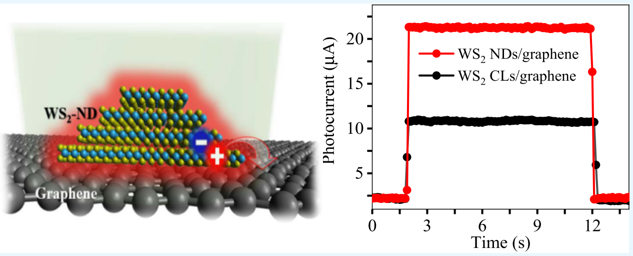

ABSTRACT: Two-dimensional material van der Waals (vdW) heterostructures provide an excellent platform for design of novel optoelectronics. In this work, transition-metal dichalcogenide WS_2 nanodiscs (WS_2-NDs) of lateral dimension of 200−400 nm and layer number of 4−7 were synthesized on graphene using a layer-by-layer, transfer-free chemical vapor deposition. On this WS_2-NDs/graphene vdW heterostructures, localized surface plasmonic resonance (LSPR) was achieved, resulting in remarkably enhanced light absorption as compared to the counterpart devices with a continuous WS_2 layer (WS_2-CL/graphene). Remarkably, the photoresponsivity of 6.4 A/W on the WS_2-NDs/graphene photodetectors is seven times higher than that (0.91 A/W) of the WS_2-CL/graphene vdW heterostructures at an incident 550 nm light intensity of 10 μW/cm^2. Furthermore, the WS_2-NDs/graphene photodetectors exhibit higher sensitivity to lower lights. Under 550 nm light illumination of 3 μW/cm^2, which is beyond the sensitivity limit of the WS_2-CL/graphene photodetectors, high photoresponsivity of 8.05 A/W and detectivity of 2.8×10^{10} Jones are achieved at V_{sd} = 5 V. This result demonstrates that the LSPR WS_2-NDs/graphene vdW heterostructure is promising for scalable high-performance optoelectronics applications.

KEYWORDS: *WS_2 nanodiscs, plasmonic, photodetectors, transfer-free, optoelectronics*

1. INTRODUCTION

Photodetectors based on two-dimensional (2D) materials, such as graphene and transition-metal dichalcogenides (TMDCs), have received considerable attention recently because of their promising electronic and optical properties. Specifically, van der Waals (vdW) heterostructures of graphene and photoactive 2D materials such as TMDCs provide a promising scheme to design high-performance photodetectors that combine the advantage of enhanced light absorption in 2D atomic layers of TMDCs and high charge mobility in graphene. For example, in the TMDC/graphene vdW heterostructure photoconductors, the TMDC layer absorbs the incident light and the generated electron−hole pairs or excitons can be dissociated to free carriers by the built-in electric field at the TMDC/graphene interface. Transferring carriers to graphene can be also facilitated by the interface built-in field, resulting in a photogating effect on graphene, and hence photoresponse as the graphene channel conductivity changes.[1] The high mobility of graphene gives rise to a very short transit time ($\tau_{transit}$) of the charge carriers within the life time of the excitons ($\tau_{exciton}$), resulting in a high photoconductive gain, which is proportional to the ratio of the $\tau_{exciton}$ and $\tau_{transit}$, up to 10^8 to 10^9.[2−5]

Various reports have demonstrated high performance of the TMDCs/graphene vdW heterostructures photodetectors.[1,6−8] The visible photoresponsivity up to 835 mA/W has been reported for a photodetector based on printed MoS_2 on transfer-free graphene.[6] The high performance of this device is attributed to a clean interface between MoS_2 and the transfer-free graphene. However, a higher photoresponsivity can be obtained by applying a gate voltage to better align the electronic structure at the vdW interface for more efficient free carrier transfer. For example, Xu et al. reported photoresponsivity of 10 A/W on the MoS_2/graphene phototransistor by application of a back-gate voltage V_{BG} = −20 V to facilitate the transfer of photo-excited holes from the MoS_2 layer to graphene.[1] This is in contrast to the lower photoresponsivity of 4.3 A/W at V_{BG} = 0 V. Interestingly, all of these TMDC/graphene heterostructure devices provide much higher performance than those based on the TMDCs or graphene only. For example, the reported responsivities are 18.8 mA/W on monolayer WS_2 photodetectors under a gate voltage of 60 V,[9] 7.5 mA/W on monolayer MoS_2 photodetectors at a gate voltage of 50 V,[10] and less than 1 mA/W on bilayer[11,12] and single-layer graphene photodetector.[13] This illustrates the unique advantage of the TMDC/graphene vdW heterostructures in achieving optimal optoelectronic process of light absorption, exciton dissociation, carrier transfer, and transport through introduction of graphene with high charge mobility.

However, light absorption in TMDC/graphene vdW heterostructures is still limited because of the small thickness of the TMDC as the photosensitizer. In fact, the limited light absorption issue represents a fundamental challenge in

Received: May 28, 2019
Accepted: August 22, 2019
Published: September 3, 2019

DOI: 10.1021/acsami.9b09262
ACS Appl. Mater. Interfaces 2019, 11, 33390−33398

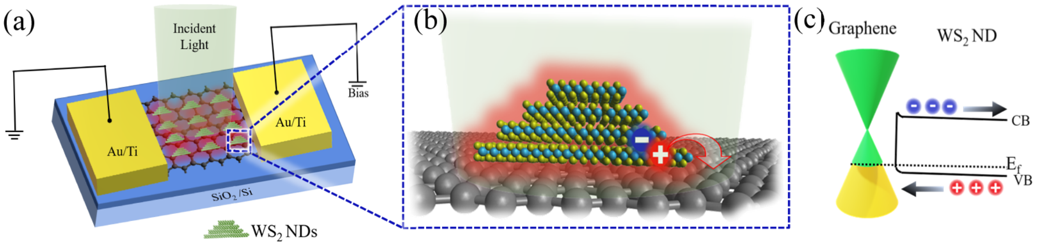

Figure 1. (a) Schematic illustration of the photodetector based on WS$_2$-NDs/graphene vdW heterostructure. (b) Zoom-in view of the WS$_2$-NDs/graphene photodetector with an illustration of the charge transfer process at the vdW interface. (c) Electronic band diagram of p-doped graphene and the WS$_2$-NDs (E_f: the Fermi level, CB: conduction band, and VB: valence band).

optoelectronic devices that only use a thin layer of sensitizer, such as quantum dots of typical diameter of a few nanometers and 2D materials of thickness in the similar range or smaller.[4−7,14−16] Development of new approaches for light trapping is therefore critical to enhance the performance of these devices. In this work, we report a novel photodetector based on a WS$_2$ nanodiscs (NDs)/graphene vdW heterostructure. We show that the WS$_2$-NDs with a lateral dimension in the range of about 200−400 nm allows localized surface plasmonic resonance (LSPR) to be generated upon light illumination and hence photo-doping, enabling enhanced light absorption and hence photoresponsivity. Furthermore, the WS$_2$-NDs were synthesized on transfer-free graphene directly grown on SiO$_2$/Si substrates using chemical vapor deposition (CVD), which is critical to obtain a clean vdW WS$_2$-NDs/graphene interface to facilitate charge transfer. On the WS$_2$-NDs/graphene photodetectors, enhanced photoresponsivity by at least seven times has been demonstrated as compared to the continuous WS$_2$ layer on graphene (WS$_2$-CL/graphene) heterostructure counterparts'. In the following, we report the experimental results.

2. EXPERIMENTAL SECTION

2.1. Transfer-Free CVD Graphene Synthesis. The synthesis of graphene was carried out into a quartz tube reactor (25 mm in diameter) inside of a horizontal CVD furnace and the details of the CVD process can be found in our previous report.[17] Briefly, a clean SiO$_2$/Si substrate was inserted into the center of the quartz tubular reactor. Then, H$_2$ (120 sccm) was introduced in the reactor while increasing the temperature until the desired temperature (1065 °C) was reached. Thereafter, CH$_4$ (30 sccm) was fed into the reactor to start graphene growth directly on the SiO$_2$/Si substrate. The growth time was maintained for 3 h. Finally, after graphene growth, the furnace was naturally cooled to room temperature under the protection of H$_2$.

2.2. Growth of WS$_2$-NDs on Graphene. The synthesis of WS$_2$-NDs was carried out on the graphene/SiO$_2$/Si substrate. A 10 mg ammonium tetrathiotungstate (NH$_4$)$_2$WS$_4$ was dissolved in 10 mL of *N*,*N*-dimethylformamide to make precursor solution with a concentration of 0.1 wt %. The solution was sonicated for 30 min for more dissolution. The SiO$_2$/Si substrate with graphene was dipped into the (NH$_4$)$_2$WS$_4$ precursor solution then the solution was spin-coated onto the graphene/SiO$_2$/Si substrate at 3000 rpm for 60 s. One dip coating followed by immediate spin coating at 3000 rpm, will result in a very thin layer of the precursor that segregated into NDs with a small diameter (~200−400 nm). Increasing the number of dipping times (~1−5 times) into the precursor leads to a different morphology for the WS$_2$ from NDs, large islands, to continuous layers. Afterward, the substrate was placed in the quartz tube CVD furnace and the temperature is raised to 450 °C under a flow of Ar/H$_2$ (40:10 sccm), and 2 g of sulfur powder was placed in the upstream of the quartz tube. The pressure was maintained at 50 mTorr. Then, the sample was annealed for about 1 h before cooling down naturally to room temperature. WS$_2$-CL was synthesized using the otherwise same procedure except the sample was dip-coated a few times (~5 times) before spin-coating. This means one-dip of the sample into the (NH$_4$)$_2$WS$_4$ precursor solution followed by immediate spinning at 3000 rpm would lead to the formation of an ultrathin precursor layer, which self-assembled into WS$_2$-NDs with a small diameter (200−400 nm) upon further annealing. With increasing number of dips to 2−3 times would lead to a thicker precursor layer and hence WS$_2$-NDs with a larger diameter. With a further increase of the number of dips, a continuous WS$_2$ of a few monolayers in thickness would form. This result indicates that the main factor to determine the morphology of the WS$_2$ is the thickness of the precursor.

2.3. WS$_2$-NDs/Graphene Photodetector Fabrication and Characterization. The metal electrodes (source and drain) of Au (40 nm)/Ti (10 nm) were deposited on graphene using electron-beam evaporation through a metal shadow mask. The distance between the electrodes (graphene channel length) is about 250 μm. Then, the substrate was dipped into the precursor solution followed with the spin-coating for a uniform layer covering the entire sample including the electrodes. Afterward, the substrate was placed in the CVD furnace for WS$_2$ growth. Raman spectra and Raman maps of graphene and WS$_2$ were collected using a Witec Alpha300-Confocal Raman microscope. Atomic force microscopy (AFM) on the same Witec system was employed to characterize the morphology and dimension of the WS$_2$-NDs. Current−voltage (I−V) characteristics of the photodetectors were measured using a CHI660D electrochemical workstation. The temporal photoresponse measurements, at 550 nm illumination with different powers and different bias voltages, were performed using an Oriel Apex monochromator illuminator.

3. RESULTS AND DISCUSSION

Figure 1a shows the schematic diagram of the WS$_2$-NDs/graphene vdW heterostructure photodetector with the source and drain electrodes. Under light illumination, the photo-excited electron−hole pairs are generated in the WS$_2$-NDs and separated at the WS$_2$-NDs/graphene interface because of the built-in electric field.[6,18] In the WS$_2$-NDs, a strong LSPR can be induced via carrier doping of semiconducting WS$_2$-NDs as depicted schematically in Figure 1b. This results in enhanced light−solid interaction and hence light absorption in WS$_2$-NDs as compared to the case of the WS$_2$-CL. Figure 1c illustrates the electronic band diagrams of the WS$_2$-NDs and the p-doped graphene at their interface. The p-type doping effect in CVD graphene is common because of adsorbed polar molecules such as H$_2$O on graphene in ambient conditions.[4,5,19] Based on the interface band diagram, the holes dissociated from electron−hole pairs are injected into graphene and the electrons remain trapped in the WS$_2$-NDs before they recombine with holes. After the transfer, the holes will drift along the graphene channel with high mobility between source and drain electrodes under a bias voltage (V_{sd}) with a short transit time $\tau_{transit}$, which is given by[2]

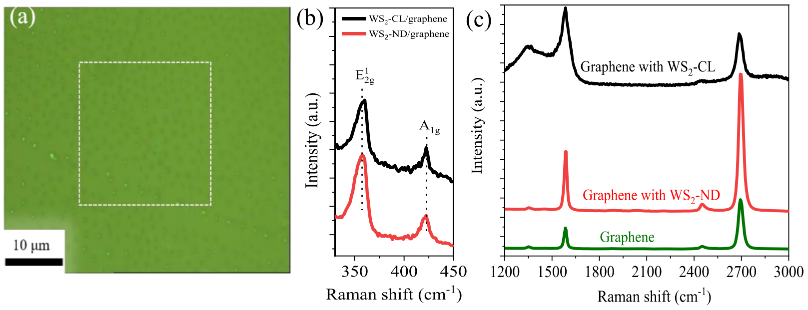

Figure 2. (a) Optical image of WS_2-NDs/graphene; (b) Raman spectra of WS_2-CL (black), and WS_2-ND (red) on graphene; (c) Raman spectra of graphene with WS_2-NDs (red), with a WS_2-CL (black), and without WS_2 (green).

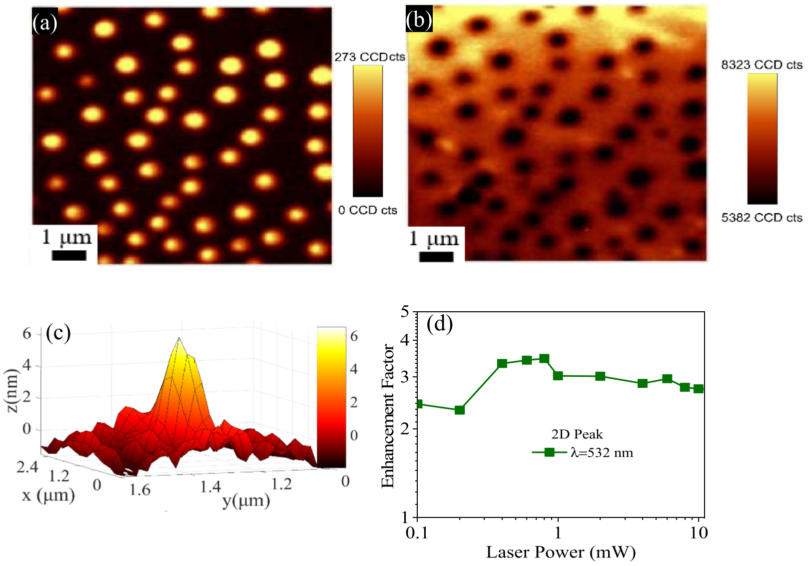

Figure 3. 10 × 10 μm^2 Raman mapping images for (a) E^1_{2g} peak of WS_2-NDs; and (b) 2D peak of graphene. The dashed square in Figure 2a is the area used for the Raman map of WS_2-NDs/and graphene; (c) 3D image for a WS_2-ND with thickness of ~5 nm and lateral dimension of ~200 nm. (d) Enhancement factor as a function of laser power using excitation lasers of 532 nm.

$$\tau_{\mathrm{transit}} = \frac{L^2}{\mu V_{\mathrm{sd}}} \tag{1}$$

where L is the graphene channel length and μ is the carrier mobility. The trapped electrons in the WS_2-NDs have the exciton lifetime τ_{exciton} that is significantly longer than the τ_{transit} because of the quantum confinement in the WS_2-NDs and high carrier mobility of graphene, allowing the holes to circulate multiple times before they recombine with electrons. Consequently, a high photoconductive gain (G) defined by[6]

$$G = \frac{\tau_{\mathrm{exciton}}}{\tau_{\mathrm{transit}}} \tag{2}$$

can be achieved.

Figure 2a displays an optical image of the WS_2-NDs/graphene vdW heterostructure. The sample looks fairly uniform in large areas. The two characteristic peaks of WS_2-NDs, at 357.16 and 421.9 cm^{-1}, are shown in the Raman spectrum (red) in Figure 2b. These two peaks correspond to the in-plane E^1_{2g} mode and out of plane A^1_g mode of WS_2.[20,21] The full width at half maximum (fwhm) of E^1_{2g} and A^1_g Raman peaks are about 18.95 and 8.55 cm^{-1}, respectively, illustrating good crystallinity with moderate defects. However, these fwhm values of WS_2-NDs are relatively larger than that reported for the crystalline exfoliated WS_2 of 11.17 and 4.67 cm^{-1},[22] which suggests the presence of growth defects in the WS_2-NDs. Consequently, the WS_2-NDs may be doped because of the presence of the defects, which may contribute to the LSPR effect as to be discussed in the following. The Raman spectrum of the WS_2-CL (black) is also included in Figure 2b. The slight blue shift of the E^1_{2g} mode to 360.26 cm^{-1} could be attributed to the smaller number of layers of the WS_2 (2−3) as opposed to that WS_2-NDs (4−7). The optical absorption spectra of the WS_2-NDs with different size and density were taken in the wavelength range of 400−900 nm. The WS_2-NDs samples with smaller sizes and higher density exhibit slightly higher absorption as shown in Figure S1c. The Raman characteristic G and 2D peaks of graphene at ~1609.00 and 2689.01 cm^{-1}, respectively, are clearly seen in Figure 2c: graphene (green), graphene with WS_2-NDs (red) and graphene with WS_2-CL (black). It should be noted that the total amount of the WS_2 material is much more in the WS_2-CL/graphene as compared to the WS_2-NDs/graphene samples because of thicker coating of the precursor in the former. The larger number of the WS_2 layer number may be attributed to the segregation of the very thin WS_2 into WS_2-NDs in the latter case. The G peak corresponds to the E^1_{2g} phonon at the Brillouin zone center and the 2D peak is the second order of the D peak that corresponds to A^1_g breathing mode.[6,23,24] The low intensity of the D peak for the graphene at 1357.12 cm^{-1} on graphene

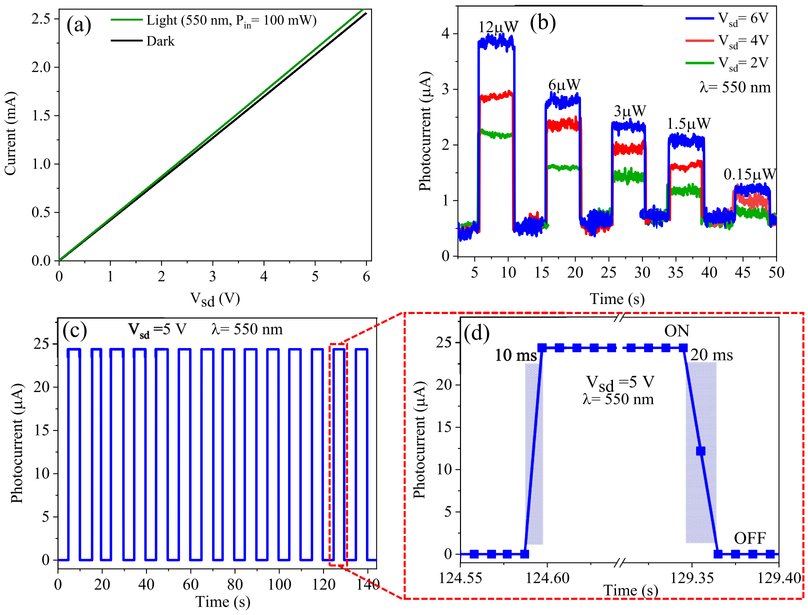

Figure 4. (a) $I-V$ characteristics measured in the dark and upon 550 nm illumination at V_{sd} = 0−6 V. (b) Photoresponse of the device at various bias voltages under various incident optical power. (c) Dynamic photocurrent measured in response to 550 nm light on and off for WS_2-NDs/graphene photodetector. (d) Enlarged part of (c).

and graphene with WS_2-NDs indicates the high quality of the transfer-free graphene that remain intact after the growth of WS_2-NDs. As shown in Figure 2c, the G and 2D peaks of graphene with the WS_2-NDs (red) are enhanced by 2.6 and 3 times, respectively, as compared to that on graphene without the WS_2-NDs (green). The enhancement is attributed to the LSPR of the WS_2-NDs similar to the LSPR of Au nanoparticles, which induces a similar enhancement of the G and 2D peaks of graphene in Au nanoparticles/graphene heterostructures.[25,26] However, no such enhancement was observed in the WS_2-CL/graphene case (black). Moreover, an enhanced D peak (defects) and a reduced I_{2D}/I_G ratio on this sample can be attributed to the interfacial interaction of graphene with WS_2-CL.[27] Figure S2 shows Raman spectra of 2D peaks of graphene of the three different samples of graphene only, WS_2-NDs/graphene and WS_2-CL/graphene. Interestingly, a blue shift of the 2D peak position from 2689.01 cm^{-1} for the graphene only to 2695.98 cm^{-1} for the WS_2-NDs/graphene sample was observed, indicating the hole-injection to graphene from WS_2-NDs. In contrast, no obvious change was observed in the position of the 2D peaks in the WS_2-CL/graphene with respect to that of the graphene only sample. While the mechanism underlying the LSPR in WS_2-NDs requires further investigation, two mechanisms are likely to contribute to the LSPR in WS_2-NDs. First, it is well known that semiconductor nanocrystals can a exhibit plasmonic effect upon carrier doping induced either via chemical composition control or/and defects.[28−30] On the other hand, the reduction of the WS_2 lateral dimension to NDs is critical as we shall discuss in the following through a comparative study of the WS_2-NDs/graphene and WS_2-CL/graphene photodetectors. Figure 3a,b displays the Raman intensity maps of the E^1_{2g} peak of the WS_2 and the 2D peak of graphene, respectively. The mapped area is marked in Figure 2a, showing the "disc-like" morphology of the WS_2-NDs with an average lateral dimension <500 nm grown on a continuous layer of transfer-free CVD graphene. Figure 3c shows an AFM image illustrating the disc-like shape, the height, and the lateral dimensions of a WS_2-ND. Based on the AFM analysis over multiple samples, the WS_2-NDs have a lateral dimension on the order of 200−400 nm, and the height of 4−5 nm. This means that the WS_2-NDs are multilayers with the layer number ranging from 4 to 7 layers of WS_2. An AFM image and a line-scan height profile over multiple WS_2-NDs on graphene are illustrated in Figure S3a,b for the analysis of the uniformity of WS_2-NDs in terms of the ND dimension and distribution. Based on the AFM analysis, the lateral and vertical dimensions of the WS_2-NDs are in the range of 200−400 and 4−5 nm, respectively. In addition, the density of the WS_2-NDs is around 3−4/μm^2. The importance of the geometry change can be illustrated in the LSPR enhancement factor that is defined as the ratio of the graphene Raman 2D peak with and without WS_2-NDs under the same Raman measurement condition. As shown in Figure 2c, no LSPR enhancement can be observed on WS_2-CL/graphene while a strong LSPR enhancement can be observed on WS_2-NDs/graphene samples. In Figure 3d, the LSPR enhancement factor of the WS_2-NDs/graphene sample was further investigated as a function of the optical power using excitation lasers of 532 nm. The enhancement of Raman signatures of analyte by metal plasmonic nanostructures has been reported by many groups, which has been used to design substrates for surface-enhanced Raman spectroscopy (SERS). Among others reported, the metal nanostructure/graphene SERS substrates have Raman enhancement due to both electromagnetic mechanism (EM) with enhancement factors up to 10^8 through LSPR on metal nanostructures and chemical mechanism with enhancement factors up to 10^3 because of charge transfer from analyte and graphene.[26,31−34] The EM depends on the evanescent electromagnetic field enhancement created at/near the surface of metal nanostructures because of collective electron oscillation on the metal surface upon light illumination. If graphene is treated as the "analyte", the Raman signatures of graphene, including both G and 2D peaks are expected to be enhanced in the metal nanostructure/graphene SERS substrates, which has been indeed confirmed experimentally using the stronger 2D peak.[25] In order to be

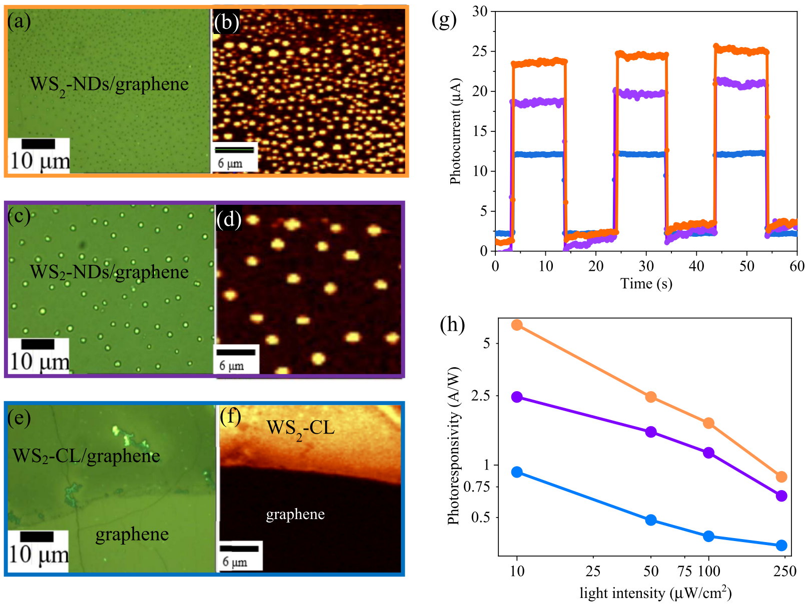

Figure 5. (a,c,e) Optical and (b,d,f) Raman mapping images of WS_2 with smaller and denser WS_2-NDs in WS_2-NDs/graphene (orange); larger and more dilute WS_2-NDs/graphene (purple) samples, and WS_2-CL/graphene (blue). (g) Corresponding dynamic photocurrents measured in response to 550 nm light on and off and (h) photoresponsivity as a function of the incident light intensity on the three devices.

consistent to quantify the LSPR effect of the WS_2-NDs on graphene, the graphene 2D peak was employed on the WS_2-NDs/graphene samples. The enhancement factor of the 2D peak of graphene has a moderate dependence on the excitation power with a shoulder observed at 0.2−0.4 mW. Below the shoulder, the enhancement factor is around 2.3−2.4 and above the shoulder, it increases with the increasing power up to ∼3.4 at 0.8 mW, followed with a slow decrease to about 2.7 at 10 mW. While further investigation is necessary, this power dependence of the LSPR enhancement factor suggests photodoping may play an important role in the LSPR effect of the WS_2-NDs.[35] Figure 4a shows the $I-V$ characteristic curve of the WS_2-NDs/graphene photodetector in the dark (black) and in response to illumination (at 550 nm) (green) with a fixed optical power of 100 mW. The illuminated current increases linearly as the bias voltage varies from 0 to 6 V because of the increase in carrier drift velocity and the decrease in transit time of the carrier between the electrodes.[36] The linear $I-V$ curve indicates an Ohmic contact between the heterostructure and electrodes. The difference between the illuminated and dark currents is defined as photocurrent ($I_{ph} = I_{light} - I_{dark}$) Figure 4b shows the dynamic photocurrent in response to light on and off at different bias voltages and different illumination powers at 550 nm. The photocurrent decreases with decreasing both the bias voltage and the power of the incident light, which is attributed to the decreased of number of photogenerated exciton (electron−hole pairs) as the incident optical power decreases from 12 to 0.15 μW. Figure 4c illustrates the dynamic photocurrent in response to multiple pulses of the 550 nm light illumination, illustrating a fast and stable photoresponse. The temporal photoresponse of the photodetector is characterized by a typical rise and fall time (t_{rise} and t_{fall}). The t_{rise} is the required time for photocurrent to rise from 10 to 90% of its maximum and the t_{fall} is the time the photocurrent takes to decay from 90 to 10%.[37] For the WS_2-NDs/graphene devices, the t_{rise} = 10 ms and t_{fall} = 20 ms at V_{sd} = 5 V is depicted in Figure 4d by the magnified part from Figure 4c, which is slightly faster than MoS_2-CL/transfer-free graphene (20−30 ms)[6] under the same conditions and also faster than MoS_2/transferred-graphene (3.2−1.2 s).[38] To elucidate the impact of the LSPR effect in the WS_2-NDs/graphene on the performance of the photodetectors, a comparative study of the photoresponse was carried out on the WS_2-NDs/graphene photodetectors with different WS_2-ND areal density and WS_2-CL/graphene photodetectors. The photodetectors are fabricated and measured under the same conditions. Figure 5a−f illustrates the optical images and Raman maps for the WS_2 on graphene: with higher WS_2-NDs areal density (a,b), lower WS_2-NDs areal density (c,d), and WS_2-CL (e,f). The dynamic photoresponse and photoresponsivity of these three samples are compared in Figure 5g,h. The highest measured values for photocurrent and the photoresponsivity (23 μA, 6.4 A/W) were observed on the WS_2-NDs/graphene sample with denser and smaller lateral size (200−400 nm). In the case of a less dense and larger size WS_2-NDs (∼500−1200 nm) shown in Figure 5c,d, the photocurrent and the photoresponsivity are decreased to 18 μA and 2.5 A/W, respectively. The lowest measured values for the photocurrent (11 μA) and the photoresponsivity (0.912 A/W) were found on the photodetector with a continuous layer of WS_2 on graphene, Figure 5e,f. The obtained values demonstrate the dependence of photocurrent and photoresponsivity on the WS_2 morphology. The photodetector with smaller and denser WS_2-NDs shows a better performance. The observed photoresponse in this work is because of the photogating effect. In the presence of the LSPR effect on the WS_2-NDs, the enhanced light absorption by the WS_2-NDs would result in higher photogating effect and hence photoresponse. We attributed the superior performance of WS_2-NDs/graphene photodetector to enhanced photogating effect because of the LSPR effect generated by WS_2-NDs. The photoresponsivity (R) is an important figure-of-merit for a photodetector and is defined as[38]

$$R = \frac{I_{ph}}{P_{in}} \quad (3)$$

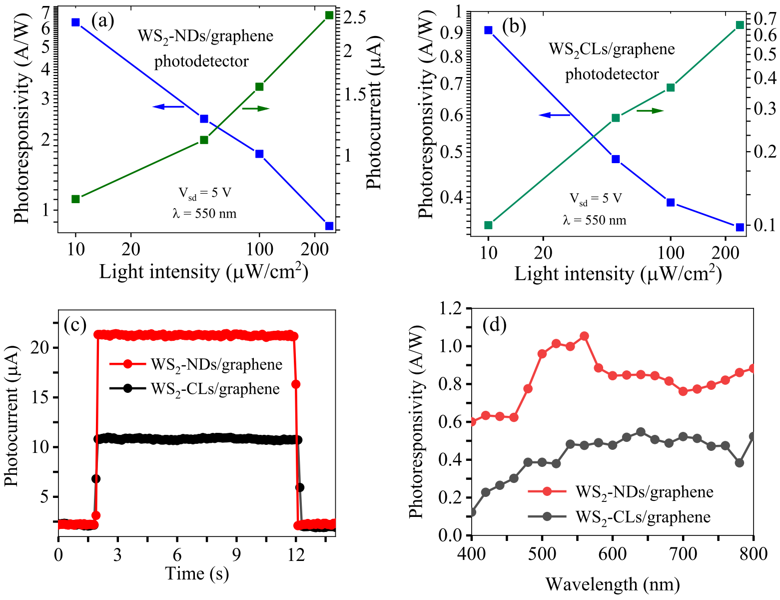

Figure 6. Photoresponsivity and photocurrent as a function of the incident light intensity of (a) WS_2-NDs/graphene heterostructure photodetector; and (b) WS_2-CLs/graphene photodetector. (c) Dynamic photoresponse of the WS_2-NDs/graphene heterostructure photodetector (red) and WS_2-CLs/graphene photodetector (black) measured in response to 550 nm. (d) Spectral photoresponsivity of the WS_2-NDs/graphene photodetector (red) and WS_2-CLs/graphene photodetector (black).

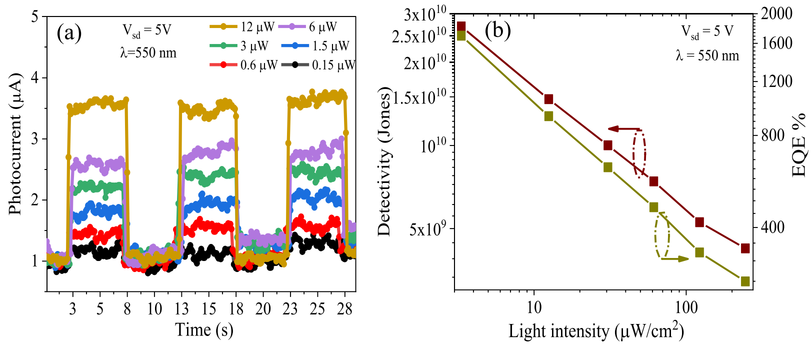

Figure 7. (a) Dynamic photoresponse of the WS_2-NDs/graphene heterostructure photodetector measured in response to 550 nm light on and off with different incident light powers; (b) Detectivity and the EQE as a function of the incident light intensity.

where P_{in} is the illumination power.

Figure 6a,b compare the R values measured on WS_2-NDs/graphene and WS_2-CL/graphene devices as a function of incident light intensity. The R values of both devices decrease monotonically with increasing incident power, while the photocurrent increases with increasing the power of incident light. The decrease in the R value is ascribed to the decreasing of charge carrier concentration which result in a lower e−h recombination.[6] At lowest power density of 10 μW/cm^2, the WS_2-NDs/graphene photodetector has a photoresponsivity of 6.4 A/W, which is seven times higher than the 0.91 A/W on the WS_2-CL/graphene counterpart. This illustrates the impact of the enhanced light absorption in WS_2-NDs as compared to the WS_2-CL. It should be noted that the R values on the WS_2/graphene vdW heterostructure photodetectors are considerably higher than that reported for WS_2 (0.0188 A/W)[9] and for graphene (0.0061 A/W).[12] Figure 6c illustrates photocurrent response of both photodetectors to light illumination (λ = 550 nm) at a bias of 5 V. The enhancement of photocurrent is clearly observed. The optimized performance of the WS_2-NDs/graphene photodetector can be attributed to the LSPR of WS_2-NDs. The spectral photoresponsivity of the WS_2-NDs/graphene and WS_2-CLs/graphene photodetectors are compared in Figure 6d. Overall, the photoresponsivity over the entire wavelength range of 400−800 nm is higher in the WS_2-NDs/graphene devices as compared to that of the WS_2-CLs/graphene. This enhanced photoresponsivity is attributed to the enhanced light absorption by the LSPR WS_2-NDs. It should be noticed that a broad peak of photoresponsivity is present at ∼500−550 nm, most probably corresponding to the LSPR wavelength of the WS_2-NDs upon photodoping. The results revealed that the LSPR WS_2-NDs can provide promising photosensitizers for enhanced performance in vdW photodetectors.

Figure 7a displays the reduction of the photocurrent as the light power decreases from 12 to 0.15 μW, measured at a 5 V bias and 550 nm illumination. The photocurrent reduction is due to the decrease of photo-generated excitons and hence free carriers. The measured external quantum efficiency (EQE) of the WS_2-NDs/graphene photodetector is illustrated in Figure 7b. The EQE can be calculated by[18]

$$\mathrm{EQE} = \frac{(I_{ph}/e)}{(P_{in}/h\nu)} \tag{4}$$

Table 1. Comparison of the Performance of Photodetectors Composed of Graphene, 2D TMDC Layers, and Their Heterostructures

device structure	V_{sd} (V)	V_{BG} (V)	R (A/W)	τ_{rise}/τ_{fall} (ms)	λ (nm)	channel length (μm)	refs
graphene	0	60	0.001		632.8	1.45	13
WS_2		20	0.0188	60/190	532	30	9
MoS_2	1	50	0.0075	50/50	550	5	10
MoS_2/graphene	0.1	−20	10	280/1500	632.8	∼20	1
MoS_2/graphene	5	0	0.835	20/30	540	250	6
$MoTe_2$/graphene	−2	0	0.02	30/30	532	∼10	8
WS_2-CLs/graphene	5	0	0.91	10/20	550	250	this work
WS_2-NDs/graphene	5	0	6.4	10/20	550	250	this work

where h is Planck's constant, ν is the frequency of incident light, and e is the electron charge. An EQE of 1800% was observed at the lowest power intensity and it decreases with increase the power intensity. The detectivity (D^*) is another figure of merit of photodetectors and it can be defined as[2]

$$D^* = \frac{A^{1/2}}{\mathrm{NEP}} = RA^{1/2}/(i_n{}^2)^{1/2} \tag{5}$$

where A is the active area of the device, NEP is the noise equivalent power, and $i_n{}^2$ is the noise current. We assume that the total noise limiting the detectivity is dominated by shot noise from I_{dark}, hence the D^* can be expressed as[18]

$$D^* = R\left[\left(\frac{A}{2eI_{\mathrm{dark}}}\right)\right]^{1/2} \tag{6}$$

where I_{dark} is the dark current. The calculated D^* for the WS_2-NDs/graphene photodetector was about 2.8×10^{10} Jones. The EQE and D^* were measured at a 5 V bias under light illumination of 550 nm with a light intensity of 3 μW/cm^2. It should be mentioned that at this low light power density of 3 μW/cm^2, the WS_2-CLs detectors did not show any measurable responses, indicating the WS_2-NDs/graphene photodetectors have larger dynamic range extending to lower light. The results have revealed that the TMDC-NDs/graphene photodetectors can improve the photodetection as compared to the previously reported on photodetectors based only on continuous 2D material sheets as well as on the TMDC-CLs/graphene photodetectors (Table 1).

4. CONCLUSIONS

In conclusion, we have successfully synthesized WS_2-NDs on transfer-free graphene using a layer-by-layer CVD process. Specifically, the WS_2-NDs with a lateral dimension of ∼200−400 nm and WS_2 layer number of 4−7 were obtained by coating a very thin layer of the $(NH_4)_2WS_4$ precursor solution followed by annealing at 450 °C under a flow of mixed gases of Ar and H_2. In contrast, a continuous layer of WS_2 was typically obtained using a thicker precursor solution layer. Photodetectors of WS_2-NDs/graphene and WS_2-CL/graphene heterostructures were fabricated and characterized in the visible spectrum. Interestingly, the lateral confinement of the electrons in WS_2-NDs leads to a strong LSPR effect as illustrated in enhanced Raman signatures of graphene by up to 3.4 in the WS_2-NDs/graphene heterostructures, which is similar to that on the metal nanoparticles/graphene heterostructures. In contrast, no such enhancement was observed on WS_2-CL/graphene. The LSPR effect enhances the photoresponse of the WS_2-NDs/graphene photodetectors considerably as compared to their counterparts based on the WS_2-CL/graphene. Under 550 nm light illumination of power intensity of 3 μW/cm^2 and bias voltage of 5 V, the WS_2-NDs/graphene photodetectors exhibited photoresponsivity of 8.05 A/W, an EQE of 1800%, and a detectivity of 2.8×10^{10} Jones. Because the light intensity of 3 μW/cm^2 is beyond the detection limit of the WS_2-CL/graphene photodetectors, the performance of the two photodetectors were compared at a higher intensity of 10 μW/cm^2 at 550 nm. The WS_2-NDs/graphene photodetectors exhibited seven-time higher photoresponsivity of 6.4 A/W than the 0.91 A/W of the WS_2-CL/graphene vdW heterostructures photodetectors. This result demonstrates the important role of the LSPR effect in enhancing the light absorption in WS_2-NDs and hence the performance of the WS_2-NDs/graphene photodetectors. Finally, the layer-by-layer transfer-free approach developed for fabrication of the WS_2-NDs/graphene heterostructures is low-cost and scalable for commercialization of high-performance optoelectronic devices.

ASSOCIATED CONTENT

Supporting Information

The Supporting Information is available free of charge on the ACS Publications website at DOI: 10.1021/acsami.9b09262.

> Raman maps of WS_2-NDs; UV−vis absorption spectra of the WS_2-NDs and Raman spectra for graphene taken from samples a and b; Raman spectra of 2D peaks positions; AFM image of WS_2-NDs; and height profile along the dashed green line with thickness of ∼4−5 nm and lateral dimension of ∼200−400 nm (PDF)

AUTHOR INFORMATION

Corresponding Authors

*E-mail: mohammed.alamri@ku.edu (M.A.).
*E-mail: jwu@ku.edu (J.Z.W.).

ORCID

Mohammed Alamri: 0000-0002-7473-8644
Brent Cook: 0000-0001-9288-7267

Author Contributions

M.A. and J.Z.W. designed the experiment. M.A. performed sample characterization. M.G., B.C., and R.G. participated in sample preparation. M.A. and J.Z.W. led the effort in manuscript writing. All authors contributed to discussions of the results and development of the manuscript.

Notes

The authors declare no competing financial interest.

ACKNOWLEDGMENTS

The authors acknowledge support in part by ARO contracts no. ARO-W911NF-16-1-0029, and NSF contracts nos. NSF-ECCS-1809293/1809284, NSF-DMR-1508494 and NSF-DMR-1909292. M.A. acknowledges the support from Umm Al-Qura University.

REFERENCES

(1) Xu, H.; Wu, J.; Feng, Q.; Mao, N.; Wang, C.; Zhang, J. High Responsivity and Gate Tunable Graphene-Mos2 Hybrid Phototransistor. *Small* **2014**, *10*, 2300−2306.

(2) Wu, L.; Qin, L.; Zhang, Y.; Alamri, M.; Gong, M.; Zhang, W.; Zhang, D.; Chan, W.-L.; Wu, J. Z. High-Sensitivity Light Detection Via Gate Tuning of Organometallic Perovskite/Pcbm Bulk Heterojunctions on Ferroelectric Pb0. 92la0. 08zr0. 52ti0. 48o3 Gated Graphene Field Effect Transistors. *ACS Appl. Mater. Interfaces* **2018**, *10*, 12824−12830.

(3) Konstantatos, G.; Badioli, M.; Gaudreau, L.; Osmond, J.; Bernechea, M.; De Arquer, F. P. G.; Gatti, F.; Koppens, F. H. L. Hybrid Graphene−Quantum Dot Phototransistors with Ultrahigh Gain. *Nat. Nanotechnol.* **2012**, *7*, 363.

(4) Zhang, W.; Chuu, C.-P.; Huang, J.-K.; Chen, C.-H.; Tsai, M.-L.; Chang, Y.-H.; Liang, C.-T.; Chen, Y.-Z.; Chueh, Y.-L.; He, J.-H. Ultrahigh-Gain Photodetectors Based on Atomically Thin Graphene-Mos 2 Heterostructures. *Sci. Rep.* **2014**, *4*, 3826.

(5) Gong, M.; Liu, Q.; Cook, B.; Kattel, B.; Wang, T.; Chan, W.-L.; Ewing, D.; Casper, M.; Stramel, A.; Wu, J. Z. All-Printable Zno Quantum Dots/Graphene Van Der Waals Heterostructures for Ultrasensitive Detection of Ultraviolet Light. *ACS Nano* **2017**, *11*, 4114−4123.

(6) Liu, Q.; Cook, B.; Gong, M.; Gong, Y.; Ewing, D.; Casper, M.; Stramel, A.; Wu, J. Printable Transfer-Free and Wafer-Size Mos2/Graphene Van Der Waals Heterostructures for High-Performance Photodetection. *ACS Appl. Mater. Interfaces* **2017**, *9*, 12728−12733.

(7) Lan, C.; Li, C.; Wang, S.; He, T.; Zhou, Z.; Wei, D.; Guo, H.; Yang, H.; Liu, Y. Highly Responsive and Broadband Photodetectors Based on Ws 2−Graphene Van Der Waals Epitaxial Heterostructures. *J. Mater. Chem. C* **2017**, *5*, 1494−1500.

(8) Kuiri, M.; Chakraborty, B.; Paul, A.; Das, S.; Sood, A. K.; Das, A. Enhancing Photoresponsivity Using Mote2-Graphene Vertical Heterostructures. *Appl. Phys. Lett.* **2016**, *108*, 063506.

(9) Lan, C.; Li, C.; Yin, Y.; Liu, Y. Large-Area Synthesis of Monolayer Ws2 and Its Ambient-Sensitive Photo-Detecting Performance. *Nanoscale* **2015**, *7*, 5974−5980.

(10) Yin, Z.; Li, H.; Li, H.; Jiang, L.; Shi, Y.; Sun, Y.; Lu, G.; Zhang, Q.; Chen, X.; Zhang, H. Single-Layer Mos2 Phototransistors. *ACS Nano* **2011**, *6*, 74−80.

(11) Xia, F.; Mueller, T.; Lin, Y.-m.; Valdes-Garcia, A.; Avouris, P. Ultrafast Graphene Photodetector. *Nat. Nanotechnol.* **2009**, *4*, 839.

(12) Mueller, T.; Xia, F.; Avouris, P. Graphene Photodetectors for High-Speed Optical Communications. *Nat. Photonics* **2010**, *4*, 297.

(13) Xia, F.; Mueller, T.; Golizadeh-Mojarad, R.; Freitag, M.; Lin, Y.-m.; Tsang, J.; Perebeinos, V.; Avouris, P. Photocurrent Imaging and Efficient Photon Detection in a Graphene Transistor. *Nano Lett.* **2009**, *9*, 1039−1044.

(14) Gong, M.; Sakidja, R.; Goul, R.; Ewing, D.; Casper, M.; Stramel, A.; Elliot, A.; Wu, J. Z. High-Performance All-Inorganic Cspbcl3 Perovskite Nanocrystal Photodetectors with Superior Stability. *ACS Nano* **2019**, *13*, 1772−1783.

(15) Levy, D.; Castellón, E. *Transparent Conductive Materials: Materials, Synthesis, Characterization, Applications*; John Wiley & Sons, 2018.

(16) Turyanska, L.; Makarovsky, O.; Svatek, S. A.; Beton, P. H.; Mellor, C. J.; Patanè, A.; Eaves, L.; Thomas, N. R.; Fay, M. W.; Marsden, A. J.; Wilson, N. R. Ligand-Induced Control of Photoconductive Gain and Doping in a Hybrid Graphene−Quantum Dot Transistor. *Adv. Electron. Mater.* **2015**, *1*, 1500062.

(17) Liu, Q.; Gong, Y.; Wang, T.; Chan, W.-L.; Wu, J. Metal-Catalyst-Free and Controllable Growth of High-Quality Monolayer and Ab-Stacked Bilayer Graphene on Silicon Dioxide. *Carbon* **2016**, *96*, 203−211.

(18) Yu, W.; Li, S.; Zhang, Y.; Ma, W.; Sun, T.; Yuan, J.; Fu, K.; Bao, Q. Near-Infrared Photodetectors Based on Mote2/Graphene Heterostructure with High Responsivity and Flexibility. *Small* **2017**, *13*, 1700268.

(19) Ryu, S.; Liu, L.; Berciaud, S.; Yu, Y.-J.; Liu, H.; Kim, P.; Flynn, G. W.; Brus, L. E. Atmospheric Oxygen Binding and Hole Doping in Deformed Graphene on a SiO_2 Substrate. *Nano Lett.* **2010**, *10*, 4944−4951.

(20) Marta, B.; Leordean, C.; Istvan, T.; Botiz, I.; Astilean, S. Efficient Etching-Free Transfer of High Quality, Large-Area Cvd Grown Graphene onto Polyvinyl Alcohol Films. *Appl. Surf. Sci.* **2016**, *363*, 613−618.

(21) Ferrari, A. C.; Basko, D. M. Raman Spectroscopy as a Versatile Tool for Studying the Properties of Graphene. *Nat. Nanotechnol.* **2013**, *8*, 235.

(22) McCreary, A.; Berkdemir, A.; Wang, J.; Nguyen, M. A.; Elías, A. L.; Perea-López, N.; Fujisawa, K.; Kabius, B.; Carozo, V.; Cullen, D. A.; Mallouk, T. E.; Zhu, J.; Terrones, M. Distinct Photoluminescence and Raman Spectroscopy Signatures for Identifying Highly Crystalline Ws 2 Monolayers Produced by Different Growth Methods. *J. Mater. Res.* **2016**, *31*, 931−944.

(23) Deokar, G.; Avila, J.; Razado-Colambo, I.; Codron, J.-L.; Boyaval, C.; Galopin, E.; Asensio, M.-C.; Vignaud, D. Towards High Quality Cvd Graphene Growth and Transfer. *Carbon* **2015**, *89*, 82−92.

(24) Barin, G. B.; Song, Y.; de Fátima Gimenez, I.; Souza Filho, A. G.; Barreto, L. S.; Kong, J. Optimized Graphene Transfer: Influence of Polymethylmethacrylate (Pmma) Layer Concentration and Baking Time on Graphene Final Performance. *Carbon* **2015**, *84*, 82−90.

(25) Zhang, S.; Zhang, X.; Liu, X. Electromagnetic Enhancement of Graphene Raman Spectroscopy by Ordered and Size-Tunable Au Nanostructures. *Nanoscale Res. Lett.* **2015**, *10*, 390.

(26) Lu, R.; Konzelmann, A.; Xu, F.; Gong, Y.; Liu, J.; Liu, Q.; Xin, M.; Hui, R.; Wu, J. Z. High Sensitivity Surface Enhanced Raman Spectroscopy of R6g on in Situ Fabricated Au Nanoparticle/Graphene Plasmonic Substrates. *Carbon* **2015**, *86*, 78−85.

(27) Alamri, M.; Sakidja, R.; Goul, R.; Ghopry, S.; Wu, J. Z. Plasmonic Au Nanoparticles on 2d Mos2/Graphene Van Der Waals Heterostructures for High-Sensitivity Surface-Enhanced Raman Spectroscopy. *ACS Appl. Nano Mater.* **2019**, *2*, 1412−1420.

(28) Luther, J. M.; Jain, P. K.; Ewers, T.; Alivisatos, A. P. Localized Surface Plasmon Resonances Arising from Free Carriers in Doped Quantum Dots. *Nat. Mater.* **2011**, *10*, 361.

(29) Gong, M.; Kirkeminde, A.; Xie, Y.; Lu, R.; Liu, J.; Wu, J. Z.; Ren, S. Iron Pyrite (Fes2) Broad Spectral and Magnetically Responsive Photodetectors. *Adv. Opt. Mater.* **2013**, *1*, 78−83.

(30) Gong, M.; Sakidja, R.; Liu, Q.; Goul, R.; Ewing, D.; Casper, M.; Stramel, A.; Elliot, A.; Wu, J. Z. Broadband Photodetectors Enabled by Localized Surface Plasmonic Resonance in Doped Iron Pyrite Nanocrystals. *Adv. Opt. Mater.* **2018**, *6*, 1701241.

(31) Qiu, H. W.; Xu, S. C.; Chen, P. X.; Gao, S. S.; Li, Z.; Zhang, C.; Jiang, S. Z.; Liu, M.; Li, H. S.; Feng, D. J. A Novel Surface-Enhanced Raman Spectroscopy Substrate Based on Hybrid Structure of Monolayer Graphene and Cu Nanoparticles for Adenosine Detection. *Appl. Surf. Sci.* **2015**, *332*, 614−619.

(32) Chen, P. X.; Qiu, H. W.; Xu, S. C.; Liu, X. Y.; Li, Z.; Hu, L. T.; Li, C. H.; Guo, J.; Jiang, S. Z.; Huo, Y. Y. A Novel Surface-Enhanced Raman Spectroscopy Substrate Based on a Large Area of Mos2 and Ag Nanoparticles Hybrid System. *Appl. Surf. Sci.* **2016**, *375*, 207−214.

(33) Alamri, M.; Sakidja, R.; Goul, R.; Ghopry, S.; Wu, J. Z. Plasmonic Au Nanoparticles on 2d Mos2/Graphene Van Der Waals Heterostructures for High-Sensitivity Surface-Enhanced Raman Spectroscopy. *ACS Appl. Nano Mater.* **2019**, *2*, 1412.

(34) Goul, R.; Das, S.; Liu, Q.; Xin, M.; Lu, R.; Hui, R.; Wu, J. Z. Quantitative Analysis of Surface Enhanced Raman Spectroscopy of

Rhodamine 6g Using a Composite Graphene and Plasmonic Au Nanoparticle Substrate. *Carbon* **2017**, *111*, 386−392.

(35) Ghopry, S. A.; Alamri, M. A.; Goul, R.; Sakidja, R.; Wu, J. Z. Extraordinary Sensitivity of Surface-Enhanced Raman Spectroscopy of Molecules on Mos2 (Ws2) Nanodomes/Graphene Van Der Waals Heterostructure Substrates. *Adv. Opt. Mater.* **2019**, *7*, 1801249.

(36) Liu, Y.; Shivananju, B. N.; Wang, Y.; Zhang, Y.; Yu, W.; Xiao, S.; Sun, T.; Ma, W.; Mu, H.; Lin, S.; Zhang, H.; Lu, Y.; Qiu, C.-W.; Li, S.; Bao, Q. Highly Efficient and Air-Stable Infrared Photodetector Based on 2d Layered Graphene−Black Phosphorus Heterostructure. *ACS Appl. Mater. Interfaces* **2017**, *9*, 36137−36145.

(37) Joshi, N. *Photoconductivity: Art: Science & Technology*; Routledge, 2017.

(38) Sun, B.; Shi, T.; Liu, Z.; Wu, Y.; Zhou, J.; Liao, G. Large-Area Flexible Photodetector Based on Atomically Thin Mos2/Graphene Film. *Mater. Des.* **2018**, *154*, 1−7.